Award numbers: 08HQGR0100 & 08HQGR0101

Locating nonvolcanic tremors and imaging their source region structure beneath the San Andreas fault, central California: Collaborative Research with the Massachusetts Institute of Technology & University of California, Berkeley

PI: M. Nafi Toksoz, co-Investigator: Haijiang Zhang

Massachusetts Institute of Technology
Dept. of Earth, Atmospheric, and Planetary Sciences
Massachusetts Institute of Technology
77 Massachusetts Avenue, 54-1816
Cambridge, MA, 02139

PI: Robert Nadeau

Berkeley Seismological Laboratory
University of California,
Berkeley, CA 94720

Final Report

October, 2009

Abstract

We analyzed tremor activity in the Parkfield region of California between 27 July 2001 and 21 February 2009. 2198 tremors (12,547 minutes of cumulative activity) were detected during our study period. Station-pair differential times were measured by cross-correlating the selected stations' root-mean-squared envelopes for all possible pair combinations having station separation distances of 100 km or less. Three different location methods were used to locate these tremors. The first one is a grid-search location method by minimizing the residuals of arrival time derived from station-pair differential times. The second one is also a grid-search location method but misfits of station-pair differential times are directly minimized to find optimal tremor locations. The 3rd one is a linearized location method directly using station-pair differential times with station corrections included. Most of the tremors were concentrated in a zone adjacent to the locked Cholame segment of the San Andreas Fault (SAF). An additional 5 to 10% were located ~65 km to the northwest along the SAF in the vicinity of Monarch Peak near Lonoak, California. Tremors in both zones occurred at depths between ~15 and 35 km: below the seismogenic zone (the upper ~15 km of Earth's crust, where most earthquakes occur) in the ductile lower crust and at or above the Mohorovicic discontinuity in this part of California.

Nonvolcanic tremors occur adjacent to locked faults and may be closely related to the generation of earthquakes. Monitoring of the San Andreas Fault in the Parkfield, California, region revealed that after two strong earthquakes, 2003 San Simeon Earthquake and 2004 Parkfield Earthquake, tremor activity increased in a nearly dormant tremor zone, increased and became periodic in a previously active zone, and has remained elevated and periodic for over 4 years. Static shear- and Coulomb-stress increases of 6 to 14 kilopascals from these two earthquakes are coincident with sudden increases in tremor rates. The persistent changes in tremor suggest that stress is now accumulating more rapidly beneath this part of the San Andreas Fault, which ruptured in the moment magnitude 7.8 Ft. Tejon earthquake of 1857.

Introduction

Nonvolcanic tremor (NVT) activity has recently been observed deep (~20 to 40 km) in subduction zones off Japan (Obara, 2002), beneath the megathrust in Cascadia (Rogers and Dragert, 2003; Szeliga et al., 2004), and along the SAF in the Parkfield-Cholame region of California (Nadeau and Dolenc, 2005). This NVT activity is characterized by low-amplitude seismic signals lasting continuously for a few minutes to several days with a predominant frequency content between 1 and 10 Hz. Unlike local and regional events, the energy content of these tremors drops off rapidly above ~10 Hz, their durations are much longer, and their amplitudes are generally smaller (Figure 1). Significant energy above 1 Hz from teleseismic events is also generally shorter in duration and is of larger amplitude. Tremors are also emergent in character and generally do not contain any clear P- or S- phase arrivals. Tremor signals generally consist of short pulsating bursts of larger amplitude energy embedded in lower amplitude activity, and at any given seismic station they are often similar in character to local cultural noise signals. Unlike cultural noise, however, tremors are observable on multiple stations, even those separated by many 10s of km, and their pulsating bursts are, to first order, coherently timed among the different stations (Figure 2). Seismic energy from tremors also appears to propagate at S-wave velocities and cross-correlation time alignments of the similarly shaped energy envelopes of the tremors have been used in an attempt to locate these events (Obara, 2002; Nadeau and Dolenc, 2005).

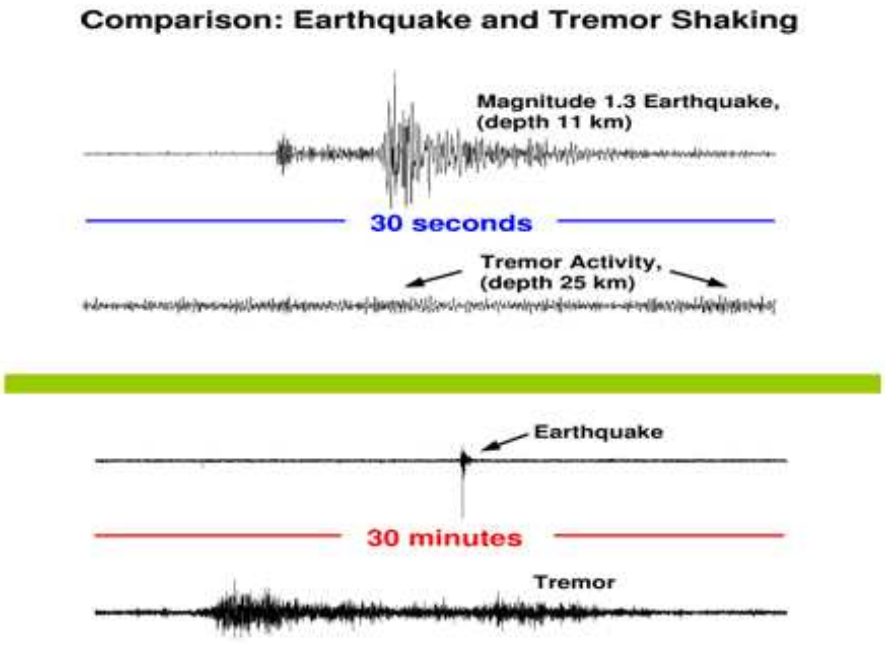

Figure 1. Contrasting properties of tremor and earthquake signals at 30 second and 30 minute time scales. In contrast to earthquake signals, tremors are of much longer duration, significantly lower amplitude and they lack clear and consistent phase arrivals.

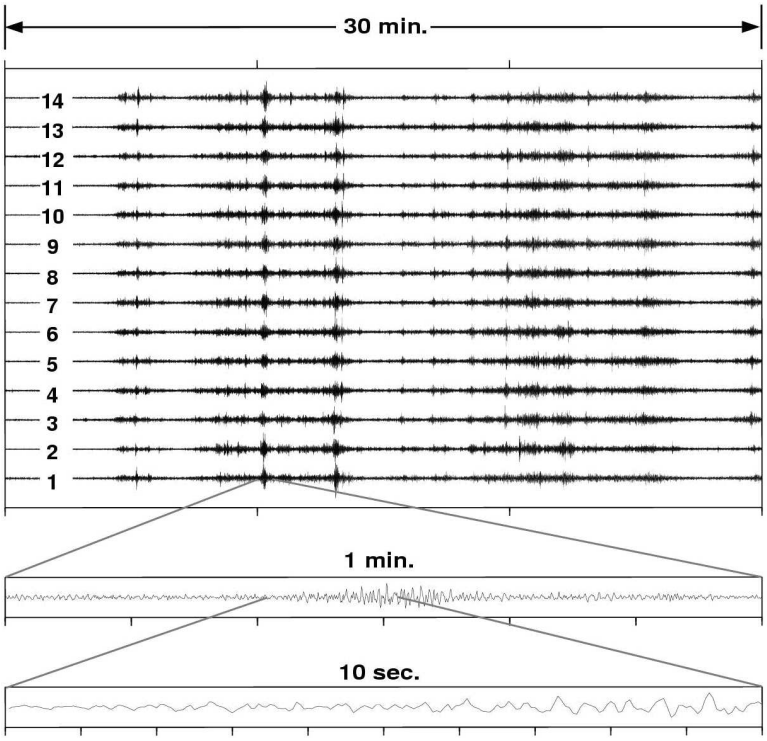

Figure 2. Seismic records of tremor activity occurring on day 341 of 2003 as recorded by horizontal components from 11 continuously recording HRSN stations (waveforms numbered 3-8 and 10-14), and 3 broad-band stations of the SCSN (1-2) and BDSN (9). Station distances from the tremor epicenter range between 20 and 50 km. Data are 20 sps records high-pass filtered at 1Hz and scaled with each record's rms amplitude. Energy bursts within the tremor are emergent in character and clear P- and S- phase arrivals are absent. Bottom 2 records are 1 min. and 10 sec. expansions of an energy burst within the tremor showing the emergent nature of these bursts and the absence of clear P- and S-phases.

Along subduction zones in Japan and Cascadia significant associations between changes in the rate of deep tremor activity, the occurrence of moderate to large earthquakes and deep slow slip events have been observed (Obara, 2002; Rogers and Dragert, 2003). More recently, apparent fore-tremor and stimulated after-tremor activity has been observed in association with the 2004 Parkfield M6 mainshock in the Parkfield-Cholame area of California (Nadeau et al., 2005). These observations suggest a significant relationship between deep (sub-seismogenic) fault zone processes associated with nonvolcanic tremor activity and the evolution and release of stress in the seismogenic crust. They also suggest that changes in tremor activity may sometimes be indicative of accelerated stressing of seismogenic fault zones by deeper sub-seismogenic deformation. However, a more complete and detailed picture of the spatial and temporal relationship between tremor activity, larger earthquakes and crustal and fault zone structure and deformation is needed to gain a better understanding of the processes giving rise to NVT and to obtain a clearer picture of their potential for indicating periods of increased stress loading and probability for larger earthquakes. The occurrence of the 28 September 2004, M6.0 Parkfield mainshock in conjunction with its associated and elevated NVT activity and the dense and now continuous seismic data coverage in the area provides a unique opportunity for investigating these issues. It will also significantly enhance our understanding of the deep rheology and deformation processes of this scientifically important and potentially hazardous fault zone.

Nonvolcanic tremors have generally been observed in transition zones between freely slipping and locked faults. In many of these locations, tremor activity increased with detectable transient fault zone deformation (slow-slip events) or with dynamic stress changes produced by solid earth and ocean tides and the surface waves of teleseismic (distant) earthquakes (Miyazawa and Mori, 2006; Gomberg et al., 2007; Rubinstein et al., 2007; Peng et al., 2008). These spatial and temporal associations suggest that tremor activity is closely related to the processes responsible for generating earthquakes. To investigate the possible relation between nonvolcanic tremors and earthquakes, we analyzed tremor activity in the Parkfield region of California between 27 July 2001 and 21 February 2009 (Figure 3). During this period, this region experienced two strong earthquakes: the moment magnitude (Mw) 6.5 San Simeon earthquake in 2003 and the Mw 6.0 Parkfield earthquake in 2004. Because of the lack of apparent P and S arrivals for the tremor signal, it is a challenge to locate tremors accurately compared to earthquakes. We here developed new location methods to locate nonvolcanic tremors directly using station-pair differential times, measured from envelope correlation of tremor signals at station pairs for one event (Obara, 2002).

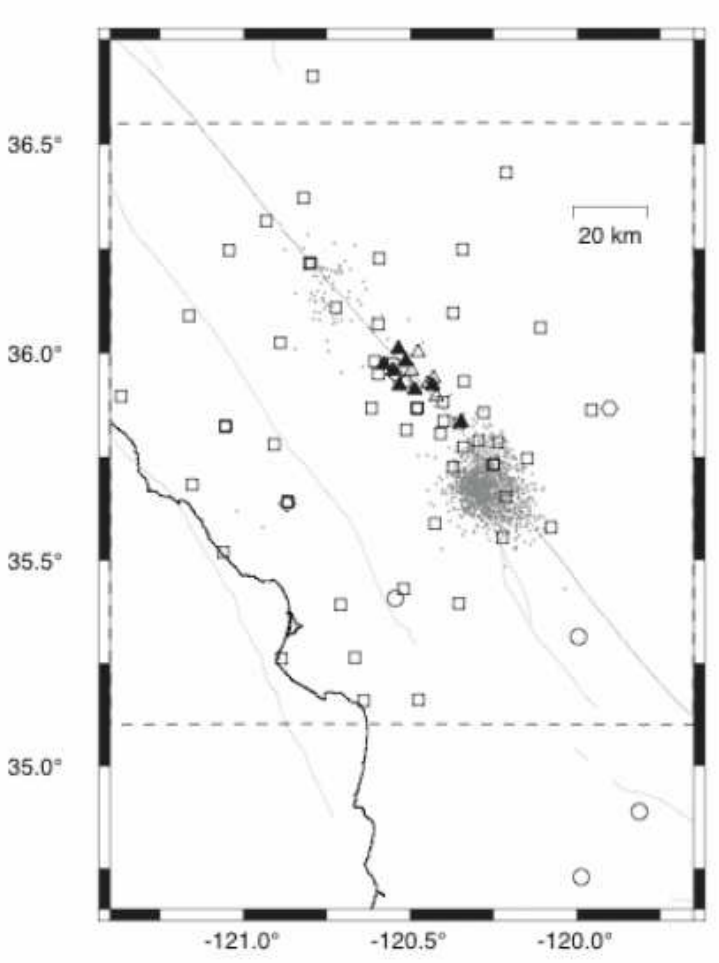

Figure 3. Seismic stations used for detecting (filled) and locating (open and filled) the tremors. Squares, triangles, circles, diamonds, and hexagon indicate stations of the NCSN (NC), HRSN (BP), SCSN (CI), BDSN (BK) and USArray (TA), respectively. Grey dots are located tremors.

Dataset

Continuously recorded seismic velocity data in the study region from 87 stations of 5 networks (i.e., High Resolution Seismic Network (HRSN, BP), Northern California Seismic Network (NCSN, NC), Berkeley Digital Seismic Network (BDSN, BK), Southern California Seismic Network (SCSN, CI), and EarthScope's USArray network (TA)) were first downloaded over the internet from the Northern and Southern California Earthquake Data Centers (NCEDC and SCEDC, respectively) (Figure 3). Short period surface sensors from the NC network were used primarily, with additional coverage provided by NC, BK, CI and TA surface broad-band and BP borehole high-frequency broad-band installations. Sampling frequencies of these data ranged from 20- to 250-Hz. The majority of stations recorded only vertical component data, so for consistency only vertical component channels were used for locating the tremors. Subsequent processing revealed that only 76 of the initial 87 channels provided data of sufficient quality for locating tremor (i.e., 56 NC, 13 BP, 4 CI, 2 BK, and 1 TA) (Figure 3).

Initial Processing

Owing to their significantly greater sensitivity compared to surface stations and their central location within the study region, data recorded continuously at 20Hz sampling frequency by 8 borehole stations of the High Resolution Seismic Network (HRSN) at Parkfield, California (Figure 3) were used for detection. One horizontal data channel from each station was used.

Gain corrections were first applied to the seismic data to account for differences among the data channels and then a 3 to 8 Hz band-pass filter was applied. Twenty-four hour root mean squared (RMS) envelope seismograms of these data were then generated using a moving 201 sample boxcar window stepped every 0.5 sec for each UTC day, yielding daily RMS seismograms with 2-Hz sampling frequency. Typical 24-hour background noise levels for each channel were also characterized by computing the channel's median RMS seismogram over 28 days and by smoothing the median seismogram with a 5-minute window to produce the channel's RMS noise signature. In general noise signatures were recomputed annually. The daily RMS seismograms for each of the data channels were then divided by that channel's 24-hour noise signature to produce signal-to-noise envelope seismograms. Division by the noise signature helps account for differences in local site attenuation and typical site-specific diurnal noise fluctuations from instrument electronics and cultural activity. The signal-to-noise seismograms are essentially a 24-hour, RMS smoothed record of the signal-to-noise ratio between daily seismic signals and typical background noise levels.

In the final processing step, 24-hour summary envelopes of the signal-to-noise seismograms were constructed for each day. This was done by computing the median amplitude of the signal-to-noise seismograms from among the stations at each 0.5 sec sample. Stations with exceptionally high variability in cultural noise levels were not included in the computation of the summary envelopes. Hence typically only 5 of the 8 stations were used.

Detection

Nonvolcanic tremor detection was carried out in 2 stages. First, initial detections were made automatically by identifying periods when the amplitude of the summary envelopes remained at or above a specified threshold for 3 minutes or longer. An amplitude threshold of 3.0 was used for data subsequent to UTC day 310 of 2003. Changes in HRSN operational parameters

phased in during UTC days 232-237 and 308-310 of 2003 improved the signal to noise of the data by approximately a factor of 1.82. To compensate for this, the amplitude threshold used prior to the HRSN parameter changes was 1.65, and during the change period thresholds of 3.0 and 1.65 were applied on a station-by-station basis.

Excluded from the analysis were data for the hours of the UTC day that followed the 22 December 2003, M 6.5 San Simeon and 28 September 2004, M 6.0 Parkfield California mainshocks and for the two days following these events. Data for these periods was dominated by amplitude transients from 1000's of frequently overlapping aftershock signals, making accurate and complete NVT detections impractical. Also excluded were 31 (of a total 2767) days of data when gaps in the HRSN continuous data streams were unacceptably high. Specifically, UTC days 264-278 of 2001; 359-360 of 2003; 364-366 of 2004; 002-004 and 007-012 of 2005; and 001 and 361 of 2006 were excluded.

The automated selection criteria were generally successful in excluding detections from most earthquakes and spurious cultural and electronic noise sources. However on occasion, amplitude transients not associated with NVT activity were also detected by the automated processing. Such transients include earthquake multiplets and swarms, unusual cultural noise signals (e.g., from deep scientific drilling activity of the San Andreas Fault observatory at Depth (SAFOD) experiment), and similarly timed multi-station artifacts that sometimes occur during network operations (e.g., severe solar regulator spiking). To remove these non-NVT transients from the automated detection list, a second stage of processing was carried out. This stage involved the visual inspection of the gain corrected and filtered seismograms from all 8 data channels and identification and exclusion of the non-NVT activity. Amplitude transients that showed artifacts or that did not show temporal coherence of primary and secondary amplitude fluctuations (pearls or bursts) lasting at least 3 minutes on at least 3 of the 8 stations were rejected. Periods of superposed NVT and earthquake activity were not rejected; however NVTs with superposed local or regional earthquakes were generally flagged as unsuitable for location. No effort was made to exclude tremors triggered by the passage of surface waves from teleseismic events.

In total 7.6 % of the automatically determined detections were excluded during the visual inspection process, leaving a total of 2198 NVT events in the detection catalog for the period July 27, 2001 through February 21, 2009. During the study period, 6 (i.e., < 0.3%) of the 2198 detected tremors were triggered by teleseismic surface waves.

Tremor Durations

The duration of each NVT is defined as the length of the NVT's detection period. Specifically, it is the length of time between the automated detection's start time (i.e., when the amplitude of the summary envelope first exceeds the detection threshold) and the detection's end time (i.e., the time following the start time when the envelope's amplitude falls below the detection threshold). Because a minimum duration of 3 minutes is required for detection, minimum NVT durations in our catalog are 3 minutes. The first, second (median), third quartiles and maximum catalog durations were 3.61, 4.65, 6.78 and 20.78 minutes, respectively. In total, 12,546.8 minutes of NVT activity were detected during the study period. However, significantly more activity typically occurs outside the detection periods at lower amplitudes, and frequently in concert with the detected tremor signals.

Station-pair differential times

The fundamental timing information used for locating the tremors was based on differential arrival time measurements of tremor signals between pairs of stations. We obtained these station-pair differential times by cross-correlating the selected stations' RMS envelopes for all possible pair combinations having station separation distances of 100 km or less. For each of the location candidates, 60 minute long snippets of vertical-component seismic data centered on the middle of the tremor detection period were extracted from the continuous data. Gain corrections, demeaning, decimation to 20Hz sampling and 3 to 8 Hz band-pass filtering were then applied. Root mean squared (RMS) envelope seismograms of these data are then generated using a moving 101 sample boxcar window stepped every 0.1 sec to yield RMS envelope seismograms with 10-Hz sampling frequency. A 2-pass, low-pass 0.070Hz filter was then applied to the RMS envelopes.

Stations whose envelopes showed anomalous amplitude fluctuations (e.g., due to glitches or spiking in the original seismic records) during the tremor detection period were excluded from the analysis. Due to the generally low seismic amplitudes of tremor signals relative to background amplitudes and to the spatial and temporal variations in background, cultural and instrumental noise levels among the stations, only envelopes from stations with good signal-to-noise levels were used. To identify stations with sufficient signal-to-noise, the 3 minute long portion of the tremor with the largest average RMS signal-to-noise was first identified based on data sweeps through data from the 6 HRSN detection stations that were least susceptible to time-varying effects. The stations that had average RMS amplitudes for the selected 3 minute time period of over 350% of background RMS amplitudes were then selected.

Six-minute windows of envelope data, centered on the 3-minute portion with the highest signal-to-noise, were used for the cross correlations. Consequently station-pair differentials for only one portion of each tremor were determined. The same 6-minute period of envelope data was used for all the stations. Differences in the arrival times between stations separated by 100 km or less are significantly smaller than the 6 minute data window length ($< \sim 10$ %) and we consider the additional error introduced into the delay times by the use of slightly different portions of the tremor energy among the station envelops to be insignificant relative to other sources of error implicit in the alignment and location processes. Only differential times with maximum cross-correlation coefficients of 0.70 or greater were used for locating the tremor.

Additional outliers in the differential-time measurements can arise due to spurious noise and culturally generated artifacts. Theoretically, the differential times between any two stations (si and sj) should be comparable to the sum of the differential times between each of the stations and a third station (sk). That is to say the differential time between a pair of stations (tsi – tsj) should equal {(tsi – tsk) + (tsk – tsj)}. We use this redundant information to identify and exclude outliers in two ways. First we remove direct-pair measurements (tsi – tsj) that differ from the median average of its 2-leg measurements {(tsi – tsk) + (tsk – tsj)} by more than 0.5 seconds. Secondly, we exclude any direct-pair measurement that involves a station that has consistently anomalous 2-leg measurements among all direct-pair/2-leg comparisons (median > 1.5 sec).

Subsequent to the data filtering and outlier removal discussed above, timing information from a median average of 25 stations per tremor remained available for locating the 2017 candidate tremors, with the minimum, first quartile, third quartile, and maximum number of stations being 2, 18, 31 and 50, respectively.

Locating nonvolcanic tremors

(1) Grid-search location method using absolute times

For each tremor, we converted the station-pair differential time measurements into a best fit set of relative arrival times for the resulting stations by choosing the station with the most cross-correlation measurements with other stations as the reference station and then performing a least squares inversion to generate arrival times relative to the reference station's arrival. Before inversion, any station pairs that were not linked (directly or indirectly) to the reference station through cross-correlation measurements were excluded. Absolute differences between the 46,638 observed and inverted station-pair differential times ranged from 0.000 to 0.780 seconds with first quartile, median and third quartile values of 0.030, 0.66 and 0.125 seconds, respectively.

Locations of the tremors were made using the migrating grid search code BW_RELP designed to locate events with sparse station coverage (Uhrhammer et al., 2001). In the location inversion, an L2-norm solution was used and we assumed that tremor energy propagates at S-velocities. The velocity model used was a gradient layer over a half space with velocities and gradients based on the regional velocity model used by the USGS for their NCSN earthquake catalog, thus allowing for more accurate comparisons of tremor and earthquake locations. Specifically, we used a surface S velocity of 2.644 km/s with a gradient down to 40 km depth of 0.05968 (km/s)/km and an S-velocity of 5.0316 km/s below 40 km.

The tremors were first located using all the available relative arrival times. If there were stations with travel-time residuals > 5 s then the station with the largest residual was identified, all station-pair differential data involving the station was removed, the best-fit relative arrival times were recomputed and the tremor was again relocated. This procedure was repeated up to 5 times if residuals > 5 seconds persisted and in the 5th iteration, all stations with residuals > 5 seconds were removed before a final location was attempted. Slightly less than 2.7% of the relative arrival time phases were removed during this large residuals exclusion process. Ten of the attempted 2017 tremor events failed to locate, leaving 2007 final locations.

Because the BW_RELP program is designed to locate events with sparse station coverage, it will locate events with very few stations and with marginal station coverage. While in some applications having locations with poor coverage and low accuracy are preferred over having no locations at all, for the purposes of resolving the general distribution of tremors in the study area we applied some additional basic criteria on location quality to generate a catalog subset of "well located" tremors. First, tremor locations that occurred at or above Earth's surface (air-tremors) or that used less than 14 phases were excluded. This reduced the catalog size by ~ 15 %. Secondly, locations with azimuthal gaps in station coverage of over 180 degrees as well as locations where depths were less than the distance to the nearest station (i.e., 45 degree depth to distance angle) were also excluded. These two basic sets of criteria reduced the final location catalog by 37.7 %, leaving 1250 tremor locations in our catalog of "well located" tremors (Figure 4). Consistent with previous spatially or temporally limited studies (Nadeau and Dolenc, 2005; Gomberg et al., 2007; Peng et al., 2008; Shelly et al., 2009), ~90% of the tremors were concentrated in a zone adjacent to the locked Cholame segment of the San Andreas Fault (SAF). An additional 5 to 10% were located ~65 km to the northwest along the SAF in the vicinity of Monarch Peak near Lonoak, California (Figure 4).

The median 95% uncertainty bounds for the well located tremors in the horizontal direction are +/- 4.7 km with 1st and 3rd quartile values of +/- 4.1 and +/- 5.5 km, respectively. In the depth direction the 95% uncertainties are +/- 4.5 km (1st and 3rd quartile, +/- 3.7 and +/- 5.2

km, respectively). Bootstrap estimates of the uncertainties are generally about twice these values, however, it is still unclear how appropriate the particular bootstrap approach we used is, considering the decidedly non-Gaussian and long-tailed distribution of the tremor residuals, the somewhat limited and heterogeneous regional-scale station coverage, the uncertainty of the dependence of the approach on the simplified velocity model in a region of strong lateral heterogeneity, the large variations among travel-path distances, and the availability of only one phase type (quasi-S) for locating the tremor.

Due to the relatively uneven station coverage and our application of a simplified velocity model in a region of strong lateral heterogeneity, the absolute position of the tremor zones, particularly with respect to the SAF boundary, are somewhat ambiguous. Tests using several plausible velocity models (i.e., with velocity contrasts across the SAF ranging between 7.5% and 15% and half space depths ranging from 20 to 50 km) suggest that the constellations of tremors in the Monarch Peak and Cholame regions could be shifted in absolute position by 3 to 5 km, though the apparent broad dimensions of the zones remain essentially the same.

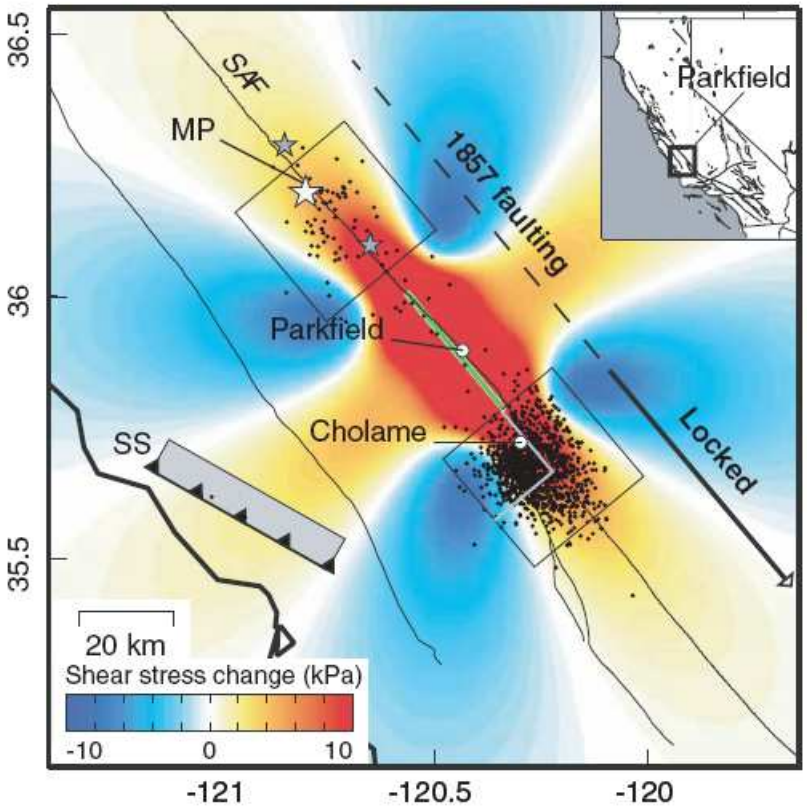

Figure 4. Study region with 1250 well-located tremors (black dots). Thirty-kilometer-square boxes (black) define the Monarch Peak (MP) and Cholame tremor zones. Color contours give regional shear-stress change at 20 km depth from the Parkfield earthquake (green segment) along the SAF. The thrust-type San Simeon earthquake rupture is represented by the gray rectangle and line with triangles labeled SS. The currently locked Cholame segment is ~63 km long (solid portion of the arrow) and is believed capable of rupturing on its own in an ~Mw 7 earthquake. The gray lines within the Cholame box bound the west quadrant, where quasiperiodic episodes predominate. The white star indicates the epicenter and the gray stars the foreshocks of the 1857 Ft. Tejon earthquake.

(2) Grid-search algorithm using station-pair differential times

For comparison, another grid-search location method is used to locate tremors but directly using the station-pair differential times. An optimal location is found to minimize the L_2 norm of the misfit between the observed and calculated station-pair differential times associated with each event. For the probabilistic location algorithm NonLinLoc, the probability density function has the form (Lomax et al., 2000; http://alomax.free.fr/nlloc/)

$$pdf(\mathbf{x}) \propto k\left[\sum_{obs_a,obs_b} \frac{1}{\sqrt{\sigma_a^{\,2}+\sigma_b^{\,2}}} \exp\left(-\frac{\{[Tobs_a(\mathbf{x})-Tobs_b(\mathbf{x})]-[TTcalc_a(\mathbf{x})-TTcalc_b(\mathbf{x})]\}^2}{\sigma_a^{\,2}+\sigma_b^{\,2}}\right)\right]^N \quad (1)$$

where $Tobs_a$ and $Tobs_b$ are the observed *arrival* times and $TTcalc_a$ and $TTcalc_b$ are the calculated travel times, respectively, for two observations obs_a and obs_b, the sum is taken over all possible pairs of observations, and N is the total number of observations. In the exponent, the first term in brackets [...] is the differential between the observed arrival times, the second term in brackets [...] is the differential between the calculated travel times, and thus the entire expression in braces {...} is the difference time between these two differentials. This expression is zero, and thus the exponential has a maximum value of 1, at points **x** where the two differentials are equal. Because the sum over observations is outside the exponential, the *pdf* has its largest values for those points X where the most pairs of observations are satisfied and thus is not sensitive to outlier data. It is also noted that the *pdf* is independent of origin time t_0.

We relocated 399 tremors for the period of 2006 to 2007 using station-pair differential times based on the same 1D S-wave velocity model used for the BW_RELP program. The RMS residual of station-pair differential times for the BW_RELP tremor locations is 2.26 s, while it is 2.22 s for the new locations. Figures 5 and 6 show the comparison of two sets of locations. The major difference between the two sets of locations is that the BW_RELP locations systematically shift to southwest and shallower. The tremor locations directly determined using station-pair differential times are mostly located deeper than 20 km. As stated above, the absolute times are derived by a least squares inversion relative to the reference station's arrival. This process may cause some systematic error in the derived absolute times. As a result, a systematic location shift may be expected.

(3) Linearized location method using station-pair differential times

In the case that we have two different stations recording a single event, we can use their differential times to locate this event, as follows:

$$\mathrm{r}_j^{\mathrm{i}} - \mathrm{r}_{\mathrm{k}}^{i} = \sum_{\mathrm{m}=1}^{3} \frac{\partial \mathrm{T}_j^{\mathrm{i}}}{\partial \mathrm{x}_{\mathrm{m}}^{\mathrm{i}}} \Delta \mathrm{x}_{\mathrm{m}}^{\mathrm{i}} + \int_{\mathrm{i}}^{j} \delta \mathrm{u}\, \mathrm{ds} - \sum_{\mathrm{m}=1}^{3} \frac{\partial \mathrm{T}_{\mathrm{k}}^{i}}{\partial \mathrm{x}_{\mathrm{m}}^{i}} \Delta \mathrm{x}_{\mathrm{m}}^{i} - \int_{i}^{\mathrm{k}} \delta \mathrm{u}\, \mathrm{ds} \quad (2)$$

where $\mathrm{r}_j^{\mathrm{i}}$ and $\mathrm{r}_{\mathrm{k}}^{\mathrm{i}}$ are residuals from event i at stations j and k, T's are travel times, x and Δx are hypocenter coordinates and their perturbations, δu is perturbation to slowness, and ds is an

element of path length. Note that the origin terms drop out since there is only one event involved. If the velocity structure is known, we only relocate this event using station-pair differential times, as follows.

$$r_j^i - r_k^i = \sum_{m=1}^{3} \frac{\partial T_j^i}{\partial x_m^i} \Delta x_m^i - \sum_{m=1}^{3} \frac{\partial T_k^i}{\partial x_m^i} \Delta x_m^i \qquad (3)$$

This method has the advantage of directly using accurate station-pair differential times and not including origin time in the inversion.

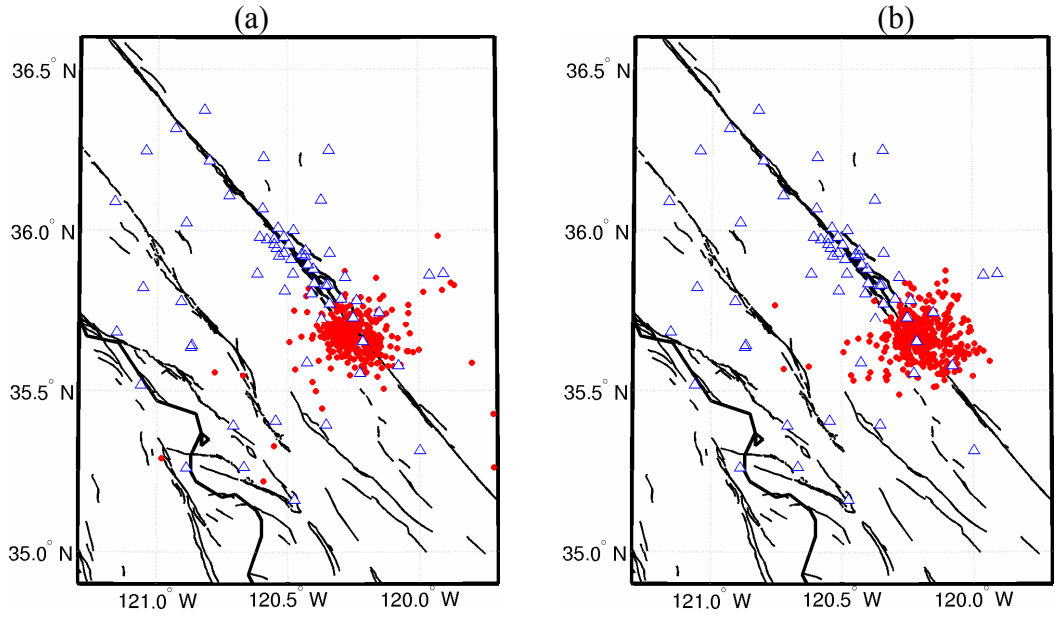

Figure 5. Comparison of the epicentral tremor locations using (a) the BW_RELP program and (b) the grid-search location method based on station-pair differential times.

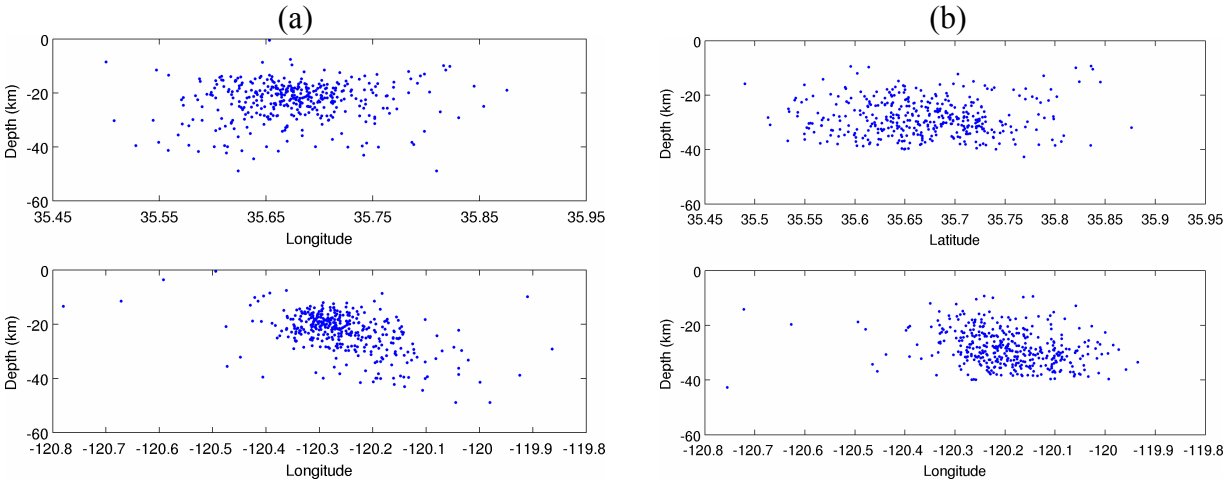

Figure 6. Comparison of tremor location depths using (a) the BW_RELP program and (b) the grid-search location method based on station-pair differential times.

We can also include station corrections in Equation (3) to account for 3D velocity heterogeneity around the stations, as follows,

$$r_j^i - r_k^i = \sum_{m=1}^{3} \frac{\partial T_j^i}{\partial x_m^i} \Delta x_m^i - \sum_{m=1}^{3} \frac{\partial T_k^i}{\partial x_m^i} \Delta x_m^i + s_j - s_k \qquad (4)$$

where s_j and s_k are station corrections for stations j and k. Figure 7 shows new tremor locations using this method. The location process starts from tremor locations determined using the grid-search location method and stops after 5 iterations. The final RMS residual is 1.33 s, a 41% decrease from the initial RMS residual of 2.22 s. In comparison, the new tremor locations are more concentrated around the San Andreas Fault and are located in the depth ranges of 20 to 35 km. Figure 8 shows the comparison of histograms of station-pair differential time residuals for grid-search location and linearized location methods. It can be seen that the station-pair differential travel time residuals both show a Gaussian-like distribution but the linearized location method shows a narrower distribution. Station corrections are greater for stations farther away from tremors. The maximum station correction is -6143 ms on station PHR located to the northernmost of tremor activity zone (Figure 7).

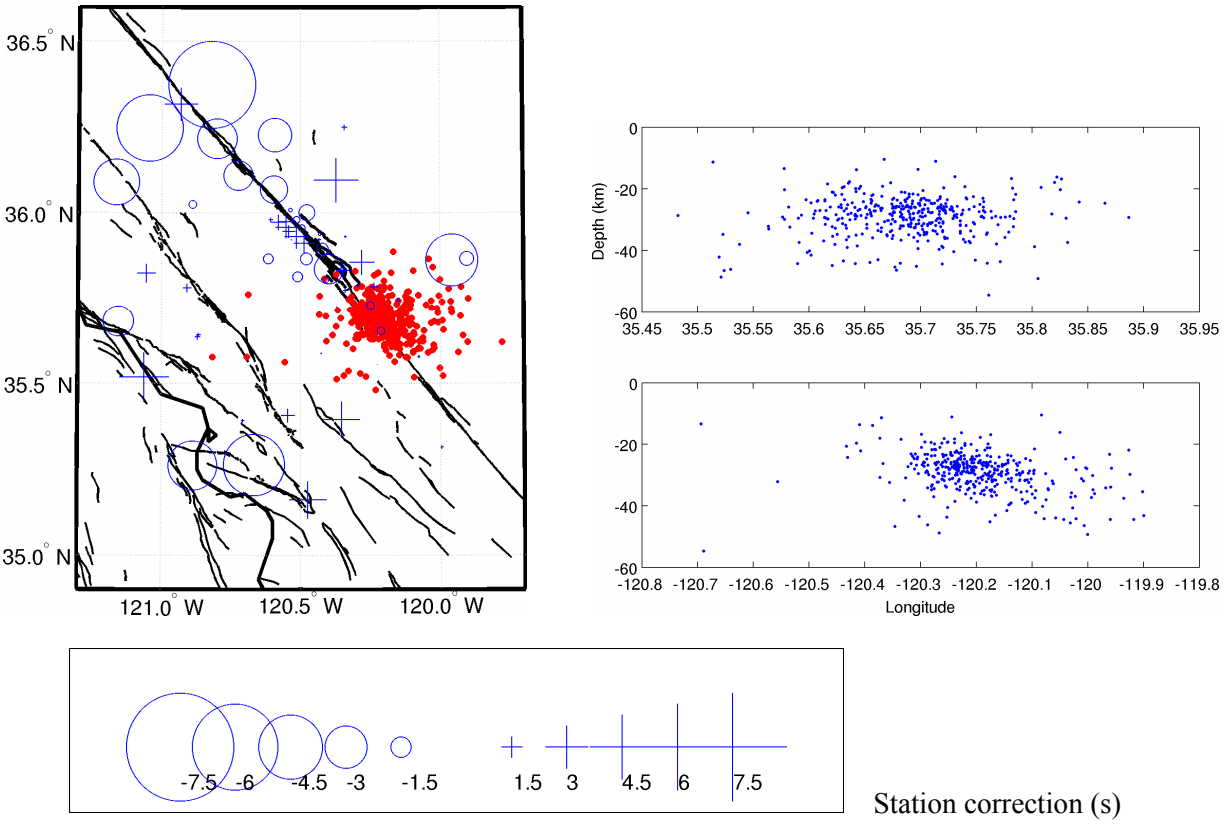

Figure 7. Tremor locations for the period of 2006-2007 using the linerized location method. In the left, positive station corrections are denoted by plus signs and negative ones are denoted by circles.

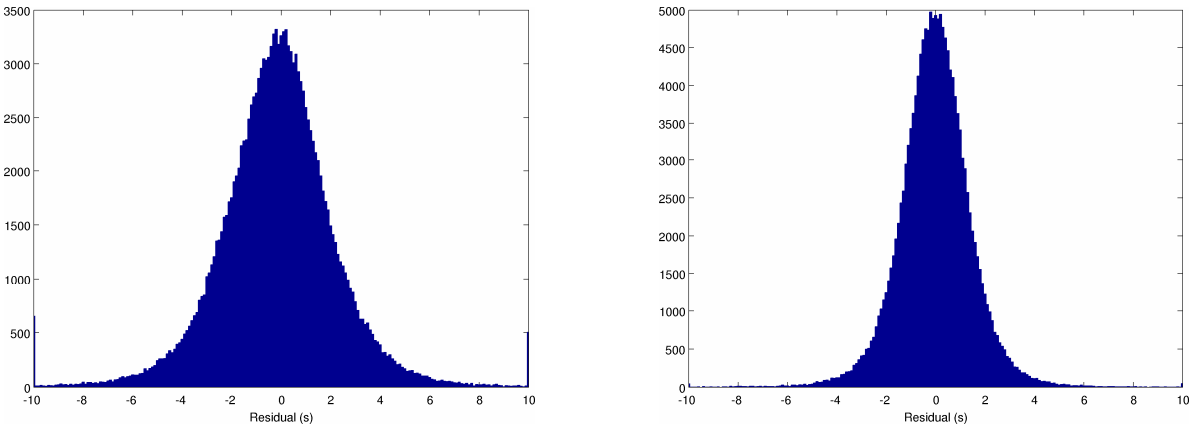

Figure 8. Histograms of station-pair travel time residuals for tremor locations from (a) grid-search location method and (b) linearized location method.

Nonvolcanic Tremor evolution and the San Simeon and Parkfield, California, Earthquakes

A sudden increase in and subsequent decay of tremor activity (aftertremors) began immediately after the 2003 San Simeon and 2004 Parkfield earthquakes (Figures 9 and 10A). Cumulatively, there was 140 min of tremor activity in the 45 days preceding the San Simeon event and 312 min of activity in the 45 days after that earthquake. An even larger increase in activity followed the Parkfield event: 850 min in the 45 days after Parkfield. In addition, approximately 3 weeks before the Parkfield earthquake, an unusually strong episode of activity (foretremor) lasting ~5 days also occurred (Figures 9 and 10A). During the 5-day episode, we detected 164 min of tremor, representing an over 10-fold rate increase as compared to the 45-day pre–San Simeon period. The peak daily activity during the episode was 82 min. The largest daily peak before the foreshock episode was 43min, occurring 98 days after the San Simeon earthquake.

The decay of tremor activity after the Parkfield event continued until mid-2006, when annual activity rates had decreased to 150% of the rate for the year preceding the San Simeon earthquake. Since mid-2006, annual rates have generally increased, reaching ~181% of the pre–San Simeon level during the final year of our analysis (Figure 10A). Our data also show that zones relatively devoid of detectable tremor can transition into a state of long-term elevated activity as a result of perturbations from a nearby moderately strong earthquake. For example, before the Parkfield earthquake, tremor activity in the Monarch Peak tremor zone (Figure 4) was low (14 tremors in ~3.2 years) (Figure 10B). However, beginning ~10 days after the Parkfield event, activity in this zone increased substantially and has continued at an elevated rate (98 tremors in ~4.4 years) (Figure 10B). The 10-day delay may reflect an anelastic redistribution of stress in the ductile lower crust. After the Parkfield earthquake, persistent episodes of quasiperiodic tremor emerged along the SAF that are reminiscent of episodic tremor observed in some subduction zones (Figure 10).

However, unlike many subduction zone tremors, where the recurrence of dominant episodes is typically 6 months or longer and is accompanied by relatively low-amplitude inter-episode activity, the SAF episodes show progressively increasing recurrence intervals ranging from ~50 days (in 2005) to ~100 days (in 2008) and are accompanied by more energetic inter-episode activity (Figure 10A). The SAF episodes have also typically occurred as bursts of activity lasting ~3 to 10 days rather than 1 to 7 weeks, as is more common in subduction zones.

These differences may, in part, be related to the tectonic environment or the much smaller dimensions of the SAF tremor zones.

The episodic tremors are not ubiquitous throughout the central part of the SAF. Rather, they seem to have been most persistent and regular in the western quadrant of the Cholame tremor zone, which is bounded by the SAF to the northeast and by the seismic-aseismic transition into the locked Cholame segment to the southeast (Figures 4 and 10B to D). This localization of tremor behavior suggests that there are differences in the process generating tremor in different subregions of the SAF. It also supports the argument that tremor in the Cholame zone is distributed both normal to and along strike of the SAF at depth. Tremors in the Cholame zone are also spatially clustered, and >55% of the tremors are separated by ≤2 km from at least four other tremors and, in some cases, from as many as 35 other events. Precise relative locations of Cholame tremor activity with waveforms similar to those of a low-frequency earthquake showed that during a 24-hour period, the similar tremor formed a deep, near-linear, SAF-parallel structure within the Cholame zone at a depth of ~26 km (Shelly et al., 2009). Taken together, the fault-normal distribution, clustering, and near-linear fault-parallel alignment of at least some tremor suggest that the SAF may broaden into several distinct subparallel zones as it extends into the ductile lower crust.

Static Coulomb- and shear-stress changes from the 2003 San Simeon and 2004 Parkfield earthquakes on planes aligned along the SAF at a depth of 20 km (Figures 4 and 11) are small in the Cholame and Monarch Peak tremor zones, but both stress types increase with increases in tremor rates in the two zones. In the Cholame zone, modeled shear- and Coulomb stress changes associated with the San Simeon earthquake are ~6 to 8 kPa, whereas those associated with the Parkfield event are ~9 to 14 kPa. In the Monarch Peak zone, shear- and Coulomb-stress changes from the San Simeon event, which failed to stimulate tremor, were negative (~ –4 to –9 kPa); however, stress changes from the Parkfield earthquake were positive (~6 to 9 kPa) and correspond to the postseismic activation in tremor activity in this zone (Figure 10B). Static normal-stress changes from the earthquakes do not clearly correspond to the tremor rate changes in either zone (Figure 11). This lack of correlation suggests that either normal-stress change did not play an important role in stimulating tremor or that other circumstances (such as the generally low change in normal stress as compared to that in shear stress, or offsetting signs of shear and normal stress) masked the effects of normal stress on tremor stimulation.

The static earthquake stress changes that stimulated the SAF tremors are roughly an order of magnitude smaller than those typically reported for the triggering of earthquakes (King et al., 1994). This suggests that tremors are a more sensitive indicator of stress change than are earthquakes. The small stress changes that stimulated the SAF tremor (~0.01 MPa or 1-10th of atmospheric pressure) are consistent with stress changes produced by solid-earth or ocean tides or the passage of surface waves from large teleseismic events that have stimulated tremor in subduction zones (Gomberg et al, 2007; Rubinstein et al., 2007; Peng et al., 2008).

The periodic tremor and persistent elevated activity after the 2004 Parkfield earthquake (Figure 10A and B) are not consistent with expectations of exponentially decaying postseismic stress after an earthquake (Savage and Langbein, 2008; Brenguier et al., 2008). It appears, therefore, that in the deep tremor zones, the SAF may have transitioned into a new state of stress and/or deformation. Models of faulting imply that step like stress perturbations from nearby earthquakes or pore pressure changes during episodic fluid release could cause deformation styles to transition between steady-state, transient, and quasiperiodic (Liu and Rice, 2007). For such mechanisms to apply to the SAF, deep slow-slip events must be occurring and fluid

pressures must be high in the tremor zones. Although deep slow slip associated with the SAF tremors has not been detected, slow-slip events with moment release equivalents as large as Mw 3 could occur in the tremor zones without being detected (Johnston, et al., 2006).

The lack of correlation between normal-stress and tremor rate changes from the San Simeon and Parkfield earthquakes may imply that effective normal stress is low and pore fluid pressure is high in the SAF zones. Recent studies of stimulation of tremor in the SAF by teleseismic events (Peng et al., 2008) and solid-earth tides (Nadeau et al., 2008) support this by showing that tremor rates correlate predominantly with variations in shear stress, even though normal-stress variations in some cases exceed shear-stress variations by roughly an order of magnitude (Nadeau et al., 2008). In subduction zones, the dehydration of subducting oceanic crust elevates fluid pressure (Shelly et al., 2006). Although subduction no longer occurs along the SAF, two strong magnetic anomalies at Monarch Peak and Cholame suggest that serpentinite bodies are present at depth, and these could be fluid sources in the tremor zones. Alternatively, deep mantle–derived fluids might also play a role (Kennedy and van Soest, 2007).

Because changes in SAF tremor activity have persisted for years beyond the last major quake in 2004, they could be signaling a shift in the process of deformation and stress accumulation beneath this portion of the SAF. The northwest tremor zone near Monarch Peak is an area of the SAF with anomalous structural complexity and low surface fault-creep rates. Two foreshocks (~Mw 6.1 and ~Mw 5.6) occurred in this area within 2 hours of the 1857Mw 7.8 Ft. Tejon earthquake (Meltzner and Wald, 1999; Toppozada et al., 2002). Faulting from the 1857 event appears to have propagated from the Monarch Peak area southeastward along the SAF for ~350 km, through Parkfield and the Cholame tremor zone (Figure 4). The rupture zone of the great 1857 event is composed of multiple fault segments, including the Cholame segment immediately southeast of the Cholame tremor zone. This segment is now fully locked. Its estimated mean recurrence time is between 85 and 142 years, and it last ruptured as part of the great 1857 event.

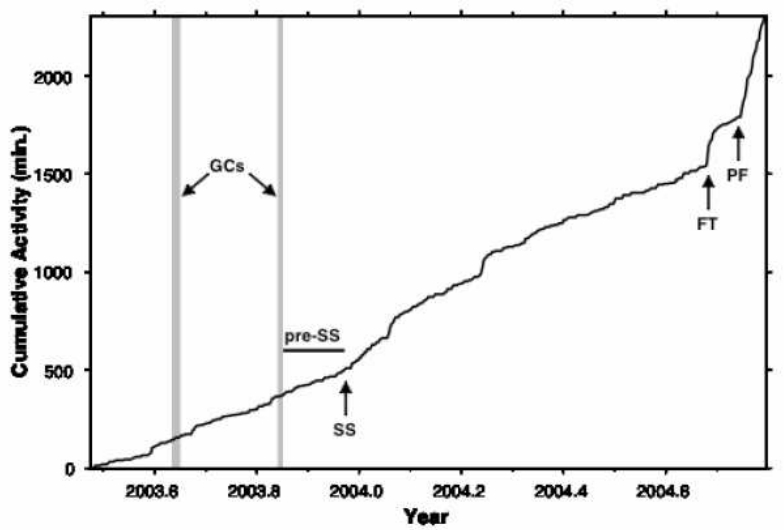

Figure 9. Cumulative tremor activity from 6 months prior to the 2003 San Simeon earthquake to 20 days after the 2004 Parkfield earthquake. Vertical grey bars (GCs) indicate the six and three day periods when changes in HRSN operational parameters where phased in. No significant variations in the rate of tremor detection are associated with these changes, indicating that the detection threshold adjustments used to correct for the changes are appropriate. SS and PF are times of the 2003 San Simeon and 2004 Parkfield earthquakes, respectively. FT indicates the 5-day fore-tremor episode that preceded the Parkfield earthquake by ~ 3 weeks.

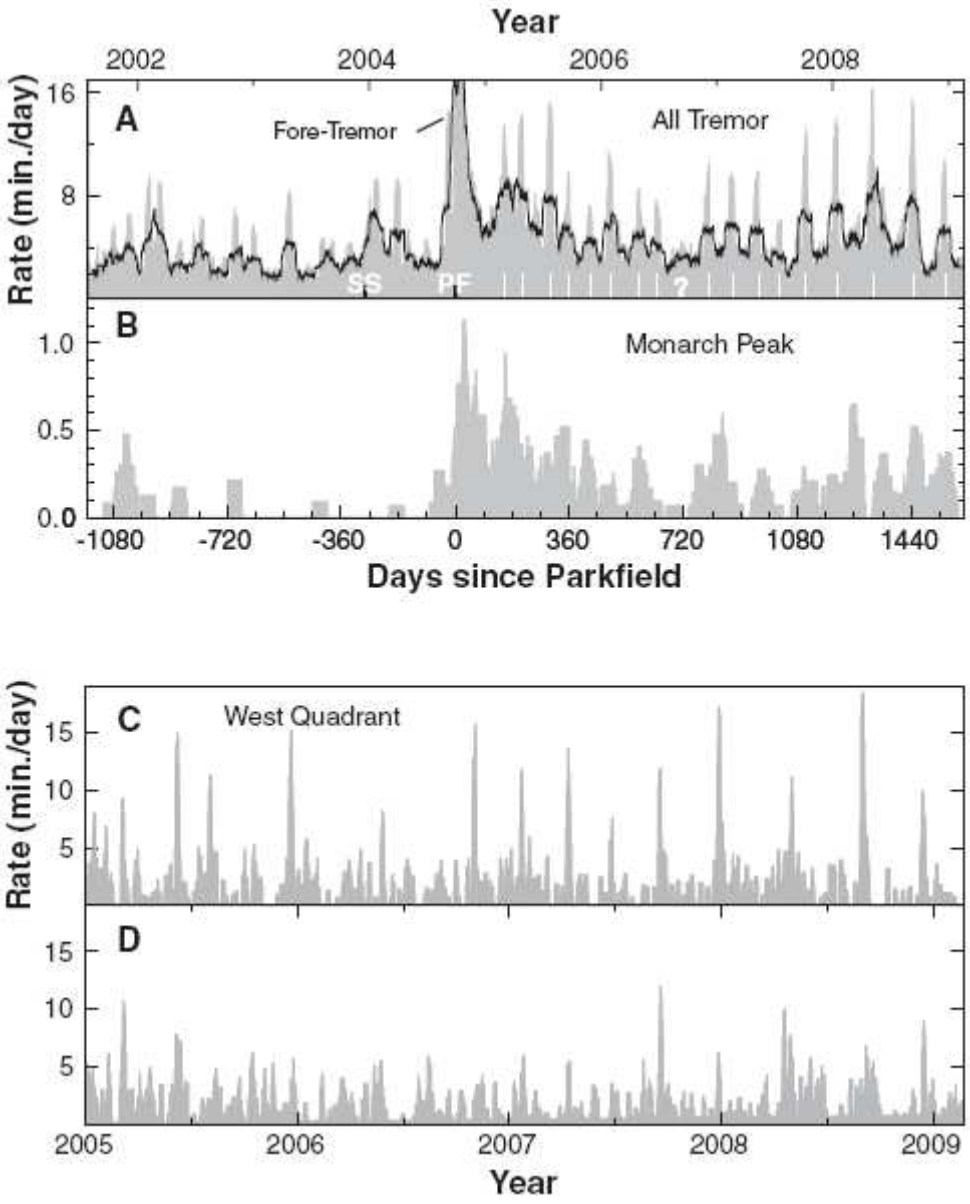

Figure 10. Time histories of tremor activity. (A) Fifteen-day (gray) and 45-day (black) smoothed rate histories for all tremors in the study area. The times of the San Simeon and Parkfield earthquakes are indicated by SS and PF, respectively. Intense foretremor activity occurred ~3 weeks before PF. Fifteen- and 45-day peak values just after PF are 31.1 and 18.9 min/day, respectively. White bars are the interpreted times of quasiperiodic episodes. The question mark is the time of a weak or missing episode. (B) History of tremor in theMonarch Peak zone (45-day smoothed rate history). (C) History since 2005 of activity (5-day smoothed) in the western quadrant of the Cholame zone (423 tremors; 2835 cumulative minutes of activity) showing strong episodic behavior. (D) Same as (C) for Cholame tremors outside the west quadrant (416 tremors; 2423 cumulative minutes), showing substantially less episodic behavior.

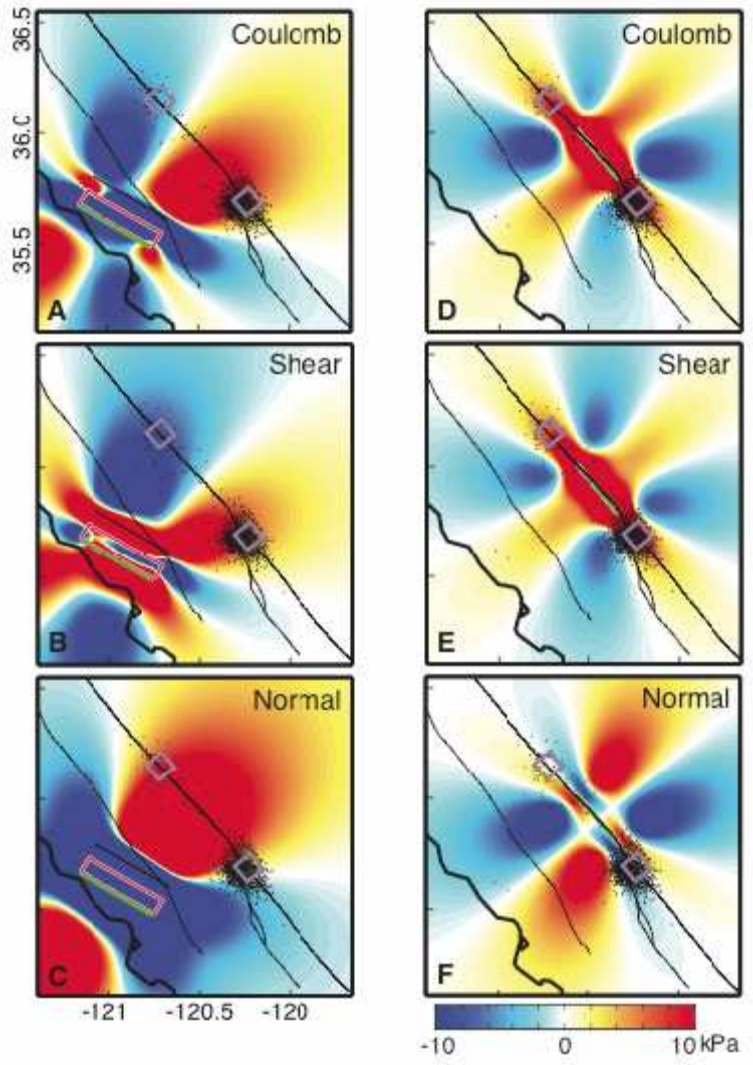

Figure 11. Calculated Coulomb- (**A**, **D**), shear- (**B**, **E**) and normal- (**C**, **F**) stress changes associated with the 2003 San Simeon (left column) and 2004 Parkfield (right column) earthquakes, respectively. The green line represents the surface trace of the two ruptures, and for San Simeon the red rectangle indicates the surface projection of its inclined (thrusting to the southwest) rupture plane. The Parkfield rupture plane was near vertical. Black dots represent the tremor locations. The purple 10-by-10 km squares are centered within the 30 km square boxes defining the Monarch Peak (northwest) and Cholame (southeast) tremor zones.

Summary

2198 nonvolcanic tremors were detected in the Parkfield region of California between 27 July 2001 and 21 February 2009. Three location methods were applied to locate tremors using station-pair differential times measured by cross-correlating the stations' RMS envelopes for all possible pair combinations having station separation distances of 100 km or less. The first two location methods are grid-search locations using either derived relative arrival times or directly station-pair differential times. The 3rd location method is a linearized location method directly using station-pair differential times with station corrections also included. The linearized location method shows great promise of improving tremor locations by directly using station-pair differential times. The tremor activity was shown to increase in a nearly dormant tremor zone, increase and become periodic in a previously active zone, and has remained elevated and periodic for over 4 years. The sudden increases in tremor rates are coincident with static shear- and Coulomb-stress increases of 6 to 14 kilopascals from the 2003 San Simeon and 2004 Parkfield earthquakes. The tremors are shown to be more sensitive to local stress changes than normal earthquakes.

Publications supported by this project

Nadeau, R. M., and A. Guilhem (2009), Nonvolcanic Tremor Evolution and the San Simeon and Parkfield, California, Earthquakes, *Science,* 325. no. 5937, 191 – 193.

Zhang, H., R. M. Nadeau, M. N. Toksoz (2009), Locating nonvolcanic tremors using station-pair differential times in the Parkfield, California region, Geophys. J. Int., in preparation.

References

Brenguier, F., Campillo, M., Hadziioannou, C., Shapiro, N. M., Nadeau, R. M. and Larose, E. (2008), Postseismic Relaxation Along the San Andreas Fault at Parkfield from Continuous Seismological Observations, *Science* **321** (5895), 1478 - 1481.

Gomberg, J., Rubinstein, J. L., Peng, Z., Creager, K. C., Vidale, J. E., and Bodin, P. (2007), Widespread Triggering of Nonvolcanic Tremor in California, *Science* **319** (5860), 173.

Ide, S., D.R. Shelly, and G.C. Beroza (2007), Mechanism of deep low frequency earthquakes: Further evidence that deep non-volcanic tremor is generated by shear slip on the plate interface, Geophys. Res. Lett., 34, L03308, doi:10.1029/2006GL028890.

Johnston, M.J.S., and R.D. Borcherdt (2005), High-resolution strain on the San Andreas Fault at Parkfield before, during and after the 28 September 2004 Parkfield Earthquake: Implications for fault response, nucleation and earthquake prediction, (abstract), Seism. Res. Lett., 76, 217, 2005.

Johnston, M.J.S., R. D. Borcherdt, A. T. Linde, and M. T. Gladwin (2006), Continuous borehole strain and pore pressure in the near field of the 28 September 2004 M 6.0 Parkfield, California, earthquake; implications for nucleation, fault response, earthquake prediction, and tremor, Bull. Seismol. Soc. Am., 96(4B):S56-S72.

Justin L. Rubinstein, Mario La Rocca, John E. Vidale, Kenneth C. Creager, and Aaron G. Wech, Tidal Modulation of Nonvolcanic Tremor, *Science* **319** (5860), 186 – 189.

Kennedy, B. M. and M. C. van Soest (2007), Flow of Mantle Fluids Through the Ductile Lower Crust: Helium Isotope Trends, *Science* **318** (5855), 1433.

King, G. C. P., R. S. Stein and J. Lin (1994), Static stress changes and the triggering of earthquakes, *Bull. Seismol. Soc. Am.*, 84, 935-953.

Lomax, A., J. Virieux, P. Volant and C. Berge (2000), Probabilistic earthquake location in 3D and layered models: Introduction of a Metropolis-Gibbs method and comparison with linear locations, in *Advances in Seismic Event Location* Thurber, C.H., and N. Rabinowitz (eds.), Kluwer, Amsterdam, 101-134.

Liu, Y., and J. R. Rice (2007), Spontaneous and triggered aseismic deformation transients in a subduction fault model, *J. Geophys. Res.*, 112, B09404, doi:10.1029/2007JB004930.

Melbourne, T.I., and F.H. Webb (2003), Slow But Not Quite Silent, Science, 300, 1886-1887.

Meltzner, A. J., and D. J. Wald (1999), Foreshocks and aftershocks of the great 1857 California earthquake, *Bull. Seismol. Soc. Am.*, 89, 1109-1120.

Miyazawa, M., and J. Mori (2006), Evidence suggesting fluid flow beneath Japan due to periodic seismic triggering from the 2004 Sumatra-Andaman earthquake, *Geophys. Res. Lett.*, 33, L05303, doi:10.1029/2005GL025087.

Nadeau, R.M., and D. Dolenc (2005), Nonvolcanic tremors deep beneath the San Andreas Fault, Science, 307, 389-389.

Nadeau, R.M., M. Traer, and A. Guilhem (2005), Repeating Earthquake and Nonvolcanic Tremor Observations of Aseismic Deep Fault Transients in Central California, EOS Trans. AGU, 86, Fall Meet. Suppl. Abstract G44A-01 (Invited).

Obara, K. (2002), Nonvolcanic deep tremor associated with subduction in Southwest Japan, Science, 296, 1679-1681.

Peng, Z., J. E. Vidale, K. C. Creager, J. L. Rubinstein, J. Gomberg, and P. Bodin (2008), Strong tremor near Parkfield, CA, excited by the 2002 Denali Fault earthquake, *Geophys. Res. Lett.*, 35, L23305, doi:10.1029/2008GL036080.

Rogers, G., and H. Dragert (2003), Episodic tremor and slip on the Cascadia subduction zone: The chatter of silent slip, Science, 300, 1942-1943.

Savage, J. C., and J. Langbein (2008), Postearthquake relaxation after the 2004 *M*6 Parkfield, California, earthquake and rate-and-state friction, *J. Geophys. Res.*, 113, B10407, doi:10.1029/2008JB005723.

Shelly, D.R., G.C. Beroza, and S. Ide (2007), Non-volcanic tremor and low-frequency earthquake swarms, Nature, 446, 305-307.

Shelly, D.R., G.C. Beroza, S. Ide, and S. Nakamula (2006), Low-frequency earthquakes in Shikoku, Japan and their relationship to episodic tremor and slip, Nature, 442, 188-191.

Shelly, D. R., W. L. Ellsworth, T. Ryberg, C. Haberland, G. S. Fuis, J. Murphy, R. M. Nadeau, and R. Bürgmann (2009), Precise location of San Andreas Fault tremors near Cholame, California using seismometer clusters: Slip on the deep extension of the fault?, *Geophys. Res. Lett.*, 36, L01303, doi:10.1029/2008GL036367.

Szeliga, W., T.I. Melbourne, M.M. Miller, and V.M. Santillan (2004), Southern Cascadia episodic slow earthquakes, Geophys. Res. Lett., 31, L16602, doi:10.1029/2004GL020824.

Toppozada, T.R., D.M. Branum, M. S. Reichle, and C. L.. Hallstrom (2002), San Andreas Fault Zone, California: $M \geq 5.5$ Earthquake History, Bull. Seismol. Soc. Am., 92, 2555-2601.

Uhrhammer, R.A., Dreger, D., and Romanowicz, B., (2001) Best practice in earthquake location using broadband three-component seismic waveform data, *Pure Appl. Geophys.*, Vol. 158, no. 1/2, pp. 259-276.